Peptide Binding by a Fragment of Calmodulin Composed of EF-Hands 2 and 3[†]

Ted M. Lakowski,[‡] Gregory M. Lee,[§] Barbara Lelj-Garolla,[§] Mark Okon,[§] Ronald E. Reid,*[,‡] and
Lawrence P. McIntosh[§,‖,⊥]

*Faculty of Pharmaceutical Sciences Division of Biomolecular and Pharmaceutical Chemistry, Department of Biochemistry and
Molecular Biology, Department of Chemistry, and The Michael Smith Laboratories, University of British Columbia, Vancouver,
British Columbia, Canada V6T 1Z3*

ABSTRACT: Calmodulin (CaM) is composed of two EF-hand domains tethered by a flexible linker. Upon
Ca^{2+}-binding, a fragment of CaM encompassing EF-hands 2 and 3 (CaM2/3; residues 46−113) folds into
a structure remarkably similar to the N- and C-domains of CaM. In this study, we demonstrate that Ca^{2+}-
ligated CaM2/3 can also bind to a peptide representing the CaM-recognition sequence of skeletal muscle
myosin light chain kinase (M13) with an equimolar stoichiometry and a dissociation constant of 0.40 ±
0.05 μM. On the basis of an analytical ultracentrifugation measurement, the resulting complex exists as
an equilibrium mixture of 2:2 heterotetrameric and 1:1 heterodimeric species. Chemical shift perturbation
mapping indicates that, similar to CaM, the peptide associates with a hydrophobic groove crossing both
EF-hands in CaM2/3. However, upon binding the M13 peptide, many residues in CaM2/3 yielded two
equal intensity NMR signals with the same ^{15}N relaxation properties. Thus, the 2:2 CaM2/3-M13 tetramer,
which predominates under the conditions used for these studies, is asymmetric with each component
adopting spectroscopically distinguishable conformations within the complex. CaM2/3 also weakly
stimulates the phosphatase activity of calcineurin and inhibits stimulation by native CaM. These studies
highlight the remarkable plasticity of EF-hand association and expand the diverse repertoire of mechanisms
possible for CaM-target protein interactions.

Calmodulin (CaM[1]) is a highly conserved, ubiquitous EF-hand protein involved in the regulation of more than 100 target proteins in response to Ca^{2+} signals (*1, 2*). Rather than a cell having many proteins, each with a Ca^{2+}-sensing domain, CaM has evolved as a common mediator that can detect a Ca^{2+} stimulus and respond by activating a diverse set of target proteins. Furthermore, the interaction between CaM and these targets is generally strong, with dissociation constants on the order of 0.01−100 nM (*3*). In this respect,

CaM is exceptional in the biological world because of its high affinity, yet broad specificity, for target recognition (*1*).

The basic principles underlying Ca^{2+} binding to CaM and its subsequent recognition of CaM-target proteins have been well established (*4−6*). CaM contains four Ca^{2+}-binding helix-loop-helix EF-hand motifs, with EF-1 and -2 associating to form its N-domain, and EF-3 and -4 forming its C-domain. The two domains are tethered through a flexible intervening linker sequence. Upon Ca^{2+} binding, the helices within each EF-hand shift from roughly antiparallel to a more perpendicular orientation, thereby exposing a hydrophobic pocket in each domain of CaM to which specific hydrophobic anchor residues in the recognition sequence of a CaM-target can bind (*6*). The flexibility of the CaM linker region allows the N- and C-domains to bind different hydrophobic residues within a variety of recognition sequences, thereby contributing to its high affinity of association with a diverse set of target proteins (*1*). These recognition sequences are often part of an auto-inhibitory domain or a pseudo-substrate motif. Thus, the activation of a downstream biological response typically results from the relief of target auto-inhibition upon CaM binding. Although target recognition generally involves both EF-hand domains of CaM, previous studies have shown that its N- and C-domain tryptic fragments of CaM can also bind to target sequences, acting as agonists or antagonists of specific CaM-stimulated enzymes (*7−10*)

Recently, we characterized a fragment of CaM composed of EF-2 and -3 (residues 46−113 (CaM2/3)) by NMR and CD spectroscopy (*11*). Upon the sequential binding of 2 equivalents of Ca^{2+} ($K_{d1} = 30 ± 5$ μM to EF-3 and a $K_{d2} >$

* To whom correspondence should be addressed. Tel: (604) 822-4706. Fax: (604) 822-3035. E-mail: calm@interchange.ubc.ca.
[‡] Faculty of Pharmaceutical Sciences Division of Biomolecular and Pharmaceutical Chemistry.
[§] Department of Biochemistry and Molecular Biology.
[‖] Department of Chemistry.
[⊥] The Michael Smith Laboratories.

[1] Abbreviations: AUC, analytical ultracentrifugation; CaM, vertebrate calmodulin; CaM2/3, residues 46−113 of vertebrate calmodulin fragment including EF-2 and -3; HSQC, heteronuclear single quantum correlation; LC-MS, liquid chromatography mass spectrometry; M13, a peptide with the sequence of residues 577−602 of skMLCK; NMR, nuclear magnetic resonance; NOE, nuclear Overhauser effect; NOESY, nuclear Overhauser effect spectroscopy; skMLCK, skeletal myosin light chain kinase; smMLCK, smooth muscle myosin light chain kinase.

1 mM to EF-2), this peptide folds into a globular, monomeric structure that is strikingly similar to both the N- and C-domains of Ca^{2+}-ligated CaM. Importantly, this folding involves the non-native pairing of EF-2 and -3, with the linker sequence of CaM now serving as a flexible loop joining these two Ca^{2+}-binding motifs. Consistent with its structural similarity to the domains of Ca^{2+}-ligated CaM, CaM2/3 possesses a solvent exposed hydrophobic groove. This suggested that CaM2/3 might also bind to and activate CaM-targets

In this study, we demonstrate that CaM2/3 can bind to a peptide (M13) representing the CaM recognition sequence of skeletal myosin light chain kinase (skMLCK). The NMR resonances from the mainchain ^1H, ^{13}C, and ^{15}N nuclei in M13-bound CaM2/3 were partially assigned using NMR spectroscopy. Although insufficient for a complete structural analysis, these assignments confirmed that the peptide binds to the hydrophobic groove of CaM2/3. However, many amides in CaM2/3 yielded double ^1H-^{15}N HSQC resonances of equal intensity upon the formation of the CaM2/3-M13 complex[2], indicating the presence of two conformations in slow exchange on the chemical shift time scale. Analytical ultracentrifugation (AUC) experiments demonstrate that this complex exists in an equilibrium between 2:2 and 1:1 complexes with a dissociation constant of 130 ± 30 μM. Therefore, at the concentrations under which the NMR experiments were performed (between 0.1 and 0.5 mM), CaM2/3-M13 exists primarily as a 2:2 heterotetramer. Furthermore, on the basis of the equal intensity double resonances, this 2:2 CaM2/3-M13 complex must be asymmetrical. In addition to binding the M13 peptide, CaM2/3 can also interact with calcineurin, as evidenced by both its ability to weakly stimulate the phosphatase activity of this enzyme and to inhibit simulation of calcineruin by native CaM. These studies exemplify the remarkable plasticity of EF-hand sequences to associate into EF-hand domains and mediate Ca^{2+}-dependent recognition of target proteins in biological signaling pathways.

EXPERIMENTAL PROCEDURES

Synthesis of the M13 Peptide. The 26 residue M13 peptide, KRRWKKNFIAVSAANRFKKISSSGAL, corresponding to the CaM recognition sequence of skMLCK, was synthesized via solid-phase peptide synthesis on an Applied Biosystems 433A peptide synthesizer (*12, 13*), cleaved (*14*), and purified by RP-HPLC according to previously described protocols (*15*). The identity of the M13 peptide was confirmed by electrospray LC-MS (observed, 2963.3 Da; predicted, 2963.5 Da) and quantitated by peptide hydrolysis followed by amino acid analysis performed with the internal standard norleucine at The Hospital for Sick Children Advanced Protein Technology Center (Toronto, Canada).

Cloning and Expression of CaM and CaM2/3. The expression vector encoding His$_6$-tagged human CaM2/3 has been described previously (*11*). The gene for vertebrate CaM was PCR-amplified from human liver cDNA (Invitrogen) with the following primers:

C G *G G A T C C* A T T G A G G G A C G C G C T G A T - CAGCTGACCGAAGAACAG and CCC*AAGCTT*GGGT-

TATCATTTTGCAGTCATCATCTGTACG. The 5′ *Bam*HI and 3′ *Hind*III DNA restriction sites are italicized, and the sequence encoding a Factor Xa protein cleavage site is underlined. A modified version of the Touchdown technique was performed in a Peltier thermal cycler (PTC-200 MJ Research) along with the primers and cDNA (*16*). The CaM gene was ligated into the pET28a+ vector using T4 DNA ligase (Invitrogen), according to the manufacturer's instructions. The final protein contained a factor Xa cleavable, N-terminal His$_6$-tag for affinity purification. The expression, purification, His$_6$-tag cleavage, and characterization of unlabeled CaM and CaM2/3 as well as ^{15}N- and $^{13}C/^{15}N$-labeled CaM2/3 were performed according to previously described protocols (*11*). All expressed proteins were quantitated by amino acid analysis as described above.

NMR Spectral Assignments of the CaM2/3-M13 Complex. Spectra were acquired at 25 °C on a 0.5 mM sample of $^{13}C/^{15}N$-CaM2/3 with 0.5 mM unlabeled M13 in NMR buffer (20 mM Tris-d_{11} (C.I.L.), 50 mM KCl, 10 mM $CaCl_2$, and $\sim$10% D_2O at pH 7.4). Note that excess $CaCl_2$ was included for all measurements to ensure saturation of both EF-2 and -3. The assignments of resonance from main chain and some side chain ^1H, ^{13}C, and ^{15}N nuclei in M13-bound CaM2/3 were established using sensitivity enhanced ^{15}N-HSQC, HNCACB, CBCA(CO)NH, H(CCO)TOCSY-NH, and ^1H-^{15}N-^1H NOESY-HSQC ($\tau_m = 150$ ms) spectra recorded on a Varian Unity 500 MHz NMR spectrometer (*17−19*). The resonances from aromatic side chain nuclei in the peptide-bound CaM2/3 were assigned with ^{13}C-HSQC, $C\beta H\delta$, and $C\beta H\epsilon$ experiments recorded on a Varian Inova 600 MHz NMR (*20*). The data were processed using NMRpipe (*21*) and analyzed using Sparky (*22*). The spectral assignments of peptide-free CaM2/3 were determined previously (*11*) and deposited in the Biological Magnetic Resonance Data Bank (accession code 7190) (http://www.bmrb.wisc.edu/).

Secondary structure predictions were obtained from $^{13}C^\alpha$ versus $^{13}C^\beta$ chemical shift differences relative to random coil values (secondary chemical shifts), calculated for each residue i in M13-bound CaM2/3 as $\Delta_{C\alpha\beta(i)} = (\delta^{13}C^\alpha_{(i)} - \delta^{13}C^\beta_{(i)}) - (\delta^{13}C^\alpha_{(coil)} - \delta^{13}C^\beta_{(coil)})$, and weighted with nearest-neighbor values, $(\Delta_{C\alpha\beta(i-1)} + 2\Delta_{C\alpha\beta(i)} + \Delta_{C\alpha\beta(i+1)})/4$, using the program CSI (*23−25*). The M13 binding site was identified from differences in the combined ^1H-$^{15}N/^{13}C$ chemical shifts between corresponding amide, aromatic, or alanine methyl groups in CaM2/3 and the CaM2/3-M13 complex, calculated as $\Delta\delta = [(\Delta\delta^1H)^2 + (\Delta\delta I(\gamma I/\gamma^1H))^2]^{0.5}$, where I is either ^{13}C or ^{15}N, and γ is the gyromagnetic ratio for the appropriate nuclei. These ratios are 26.75, -2.71, and 6.73×10^7 rad T^{-1} s^{-1} for ^1H, ^{15}N, and ^{13}C, respectively.

NMR-Monitored Titration of CaM2/3 with M13. The binding of unlabeled M13 peptide to ^{15}N-CaM2/3 was monitored with sensitivity enhanced gradient ^{15}N-HSQC spectra run at 25 °C on a Varian Inova 600 MHz spectrometer. A total volume of 85 μL of 1.8 mM M13 peptide in NMR buffer was added in 5 or 10 μL aliquots to a sample of ^{15}N-CaM2/3, initially at 0.18 mM in 0.48 mL of the same buffer. At the end of the titration, there was a 1.8:1 molar ratio of M13:^{15}N-CaM2/3. The data were analyzed by plotting ^{15}N-CaM2/3 amide peak intensity, after correction for dilution, versus the concentration of added M13, followed

---

[2] All complexes are Ca^{2+}-ligated unless stated otherwise.

by fitting to a single site binding model using the program CaLigator (*26*).

Backbone ^{15}N Relaxation of the CaM2/3-M13 Complex. Backbone amide ^{15}N relaxation parameters were acquired for 0.5 mM M13-bound $^{13}C/^{15}N$-CaM2/3 at 25 °C using a Varian Unity 500 MHz NMR spectrometer (*27, 28*). Data points for the T_1 (10 to 1053.5 ms) and T_2 (16.7 to 166.0 ms) experiments were collected in random order. Steady-state heteronuclear $^1H\{^{15}N\}$NOE spectra were acquired with and without 2 s of ^1H saturation and a total recycle delay of 5 s. All data were processed with NMRpipe (*21*) and T_1 and T_2 lifetimes obtained by fitting to a single-exponential decay using Sparky (*22*). Errors for heteronuclear $^1H\{^{15}N\}$NOE ratios were estimated according to previously described methods (*28*). The effective correlation time for isotropic rotational diffusion (τ_c) of the CaM2/3-M13 complex and the model-free order parameters (S^2) for the backbone amides of bound CaM2/3 were calculated with Tensor 2.0 (*29*). Residues for which the $^1H\{^{15}N\}$NOE ratios were <0.6 and for which the values of $[(\langle R_2 \rangle - R_{2i})/\langle R_2 \rangle) - (\langle R_1 \rangle - R_{1i})/\langle R_1 \rangle)]$ were >1.5 times the standard deviation of this difference were excluded from the τ_c calculations because of the possibility of fast internal motions or chemical exchange broadening (*30*).

Analytical Ultracentrifugation. Sedimentation velocity experiments were conducted at 20 °C with a Beckman Optima XL-I analytical ultracentrifuge equipped with both absorbance and interference optics. Standard aluminum double-sector centerpieces (12 mm) were filled with protein solution (400−450 μL), in a buffer composed of 20 mM Tris HCl, 50 mM KCl, and 10 mM $CaCl_2$ at pH 7.4. The solutions contained 1:1 mixtures of M13 and CaM2/3, each at 38, 75, or 150 μM. Buffer was also placed in the reference cell. The loaded cells were thermally equilibrated in the centrifuge for at least 1 h after the instrument had reached 20 °C under vacuum. The rotor speed was then set to 50,000 rpm, and radial absorbance scans were acquired with 0.003 cm steps in continuous mode without averaging.

Sedimentation equilibrium experiments were performed at 20 °C with a 6-channel Epon centerpiece in 4-hole (AnTi60) and 8-hole (AnTi50) rotors. The buffered solutions contained CaM2/3 or M13 at 20, 40, or 75 μM, or 1:1 mixtures of CaM2/3 and M13, each at 38, 75, or 150 μM. The rotor speed was set at 20,000, 30,000, or 50,000 rpm, and 5 radial interference scans were acquired with 0.001 cm steps and subsequently averaged. Sample equilibration was verified with WinMatch (*31*).

The solution densities and partial specific volumes were calculated with SEDNTERP (*32*). SEDPHAT (*33*) was used for the analysis of the equilibrium experiments. Velocity data were analyzed with SEDPHAT producing a c(s) distribution of the solution of the Lamm equation, calculated with SEDFIT (*34*), assuming the regularization parameter p to be 0.95. Sedimentation coefficient increments of 200 were used in the appropriate range for each sample.

Calcineurin Stimulation Assay. The stimulation of calcineurin (protein phosphatase-2B or PP-2B) by both CaM and CaM2/3 was assessed in 96 well plate format by measuring phosphatase activity against *p*-nitrophenol phosphate (pNPP). The reaction buffer was composed of 50 mM Tris at pH 7.0, 1 mM $CaCl_2$, 1 mM $NiCl_2$, and 0.125 mg/mL BSA. Samples with calcineurin alone as well as

calcineurin with CaM2/3 or CaM were preincubated at 37 °C for 30 min. The reaction was initiated by the addition of pNPP, in reaction buffer, to a final concentration 0.9 mg/mL. The appearance of nitrophenol was quantitated with a Labsystems Multiskan Ascant plate reader at 405 nm (*35, 36*). Initial rates were measured from reactions with 50 nM (0.70−0.74 μg) calcineurin, and CaM or CaM2/3 at concentrations of 0, 5, 10, 25, 50, 100, and 300 nM per reaction. A competition assay was also performed with 0, 10, 50, and 300 nM CaM samples containing 0, 10, 50, and 100 nM CaM2/3.

RESULTS

Binding of M13 to CaM2/3 Measured by NMR-Monitored Titrations. The interaction between Ca^{2+}-saturated ^{15}N-CaM2/3 and M13 was investigated by ^{15}N-HSQC spectroscopy. The chemical shifts and relaxation properties of an amide are highly sensitive to even subtle conformational changes such as those occurring at interaction surfaces. Thus, shift perturbations in NMR-monitored titrations can be used to qualitatively identify binding interfaces and to quantitatively measure binding affinities. Upon the incremental addition of M13, a progressive disappearance of the amide ^1H-^{15}N signals from unbound CaM2/3 was observed, along with concomitant appearance of a new set of signals (Figure 1). These signals, which arise from the CaM2/3-M13 complex, indicate that binding occurs in the slow exchange limit on the chemical shift time scale (i.e., the rate of exchange between free and bound states is less than the frequency differences for corresponding amides in each state).

A striking feature of the ^{15}N-HSQC spectrum of M13-saturated CaM2/3 is the appearance of more amide signals than expected and observed with free CaM2/3. Using conventional ^1H-^{13}C-^{15}N correlation experiments recorded on an equimolar complex of $^{15}N/^{13}C$-CaM2/3 with unlabeled M13, resonances from the main chain nuclei of the labeled protein were assigned. As summarized in Figure 1, 33 out of 63 non-proline residues in M13-bound CaM2/3 yielded two resolved amide $^1H^N$-^{15}N peaks of equal intensity, arbitrarily denoted as 'a' and 'b'. Similarly, additional peaks were observed in the ^{13}C-HSQC spectrum of the labeled protein. Two resolved indole $^1H^{\epsilon 1}$ signals of equal intensity from the sole tryptophan in M13 were also present in the ^1H NMR spectrum of the CaM2/3-M13 complex (not shown). Thus, CaM2/3-M13 must adopt at least two distinguishable conformations of very similar or identical populations. Unfortunately, because of spectral degeneracy, we were unable to specifically determine which of the 'a' and 'b' signals for a given amide corresponds to which conformation of the bound CaM2/3. That is, many residues with two amide signals still had similar $^{13}C^\alpha$ and $^{13}C^\beta$ shifts at the recorded spectral resolution, reflecting the generally lower sensitivity of aliphatic resonances versus amide resonances to conformational perturbations. Also, because of spectral complexity, we were unable to confidently assign the resonances from the unlabeled M13 peptide (except for its indole $^1H^{\epsilon 1}$) using $^{15}N/^{13}C$-filtered ^1H-^1H TOCSY and NOESY experiments in which signals from $^{15}N/^{13}C$-CaM2/3 were suppressed. Finally, we did not detect the transfer of magnetization between the 'a' and 'b' peaks of any given amide in ^1H-^{15}N-^1H NOESY-HSQC and HSQC-monitored N_z exchange experiments (not shown) (*37*). Thus, any exchange between the

FIGURE 1: Ca^{2+}-loaded CaM2/3 binds the M13 peptide in two conformations. Shown is the assigned ^{15}N-HSQC spectrum of ^{15}N-CaM2/3 with unlabeled M13 in a 1:1.8 molar ratio (red), superimposed upon that of free ^{15}N-CaM2/3 (green), recorded at 25 °C and pH 7.4. Many CaM2/3 amides in the complex yield two resolved $^{1}H^{N}$-^{15}N signals of equal intensity, denoted as 'a' (downfield in ^{1}H) and 'b' (upfield). The residues are numbered according to the sequence of CaM, and the inset corresponds to the central boxed region of the spectrum. The signals from the unbound protein (*11*) generally fall near those of the bound protein and are not labeled for clarity. The horizontal lines connect resonances from the glutamine or asparagine side chain $^{15}NH_2$ groups.

bound states of the CaM2/3-M13 complexes, either intramolecularly or via dissociation to free M13 and CaM2/3, occurs on a time scale slower than their $^{1}H^{N}$ or ^{15}N T_1 values (i.e., seconds).

A quantitative analysis of the titration of CaM2/3 with the M13 peptide is presented in Figure 2. On the basis of a plot of the average normalized intensities of the amide $^{1}H^{N}$-^{15}N peaks from residues 48−55, 65−92, and 102−113 within the helical and linker regions of bound CaM2/3, saturation occurs at an equimolar CaM2/3/M13 ratio (Figure 2A). However, as demonstrated below, this corresponds to a 2:2 heterotetrameric complex. Fitting of these titration data to a model describing the equilibrium CaM2/3 + M13 ⇌ CaM2/3-M13 yielded an apparent K_d of 0.40 ± 0.05 μM. Note that this value, which is consistent with relatively high affinity association in the slow exchange regime, reflects the formation of all bound species and the assumption of equivalent binding sites in the 2:2 complex. Figure 2B also plots the absolute intensities from three residues showing double resonances F65 (F65a and b), I100 (I100a and b), and L105 (L105a and b) versus the concentration ratio of added M13 to ^{15}N-CaM2/3. Over the entire titration experiment, the observed double peaks of these, and all other amides (not shown), are of nearly equal intensity. Hence, the two NMR-distinguishable conformations of the CaM2/3-M13 complex are isoenergetic, forming with the same binding affinity.

Analytical Ultracentrifugation of the CaM2/3-M13 Complex. Analytical ultracentrifugation (AUC) was used to

further investigate the stoichiometry of the CaM2/3-M13 complex. Sedimentation velocity and equilibrium data were obtained for CaM2/3, M13, and CaM2/3-M13 in the presence of excess Ca^{2+} at 20 °C. As summarized in Figure 3, the M13 peptide (75 μM) sedimented as an essentially monodisperse species with a sedimentation coefficient of 0.48 S. Consistent with this value, a global fit of the sedimentation equilibrium experiments, performed at three different concentrations, confirmed that the M13 peptide is monomeric under these experimental conditions (apparent MW = 2810 Da; theoretical = 2963 Da). In contrast, fitting of the sedimentation velocity data measured for CaM2/3 (75 μM) revealed a major 1.3 S species, as well as a minor ∼2.4 S species (6%) attributable to monomeric and dimeric forms of the protein, respectively. Sedimentation equilibrium analysis confirmed that CaM2/3 has a weak tendency to dimerize (K_d ∼ 4 mM). Therefore, at submillimolar concentrations, CaM2/3 is predominantly monomeric, as demonstrated previously through NMR structural and dynamic studies (*11*).

Sedimentation velocity data were also recorded for the complex of CaM2/3 and M13 (each at 38, 75, or 150 μM). Given the apparent K_d for complex formation of 0.40 μM, >90% of CaM2/3 and M13 should be in the bound form under the conditions of these experiments. For each sample, the fit c(s) distribution revealed a major species with a sedimentation coefficient of 2.1 S (Figure 3). This sedimentation coefficient is larger than that expected for a 1:1 CaM-M13 complex, but smaller than that for a 2:2 heterotetramer.
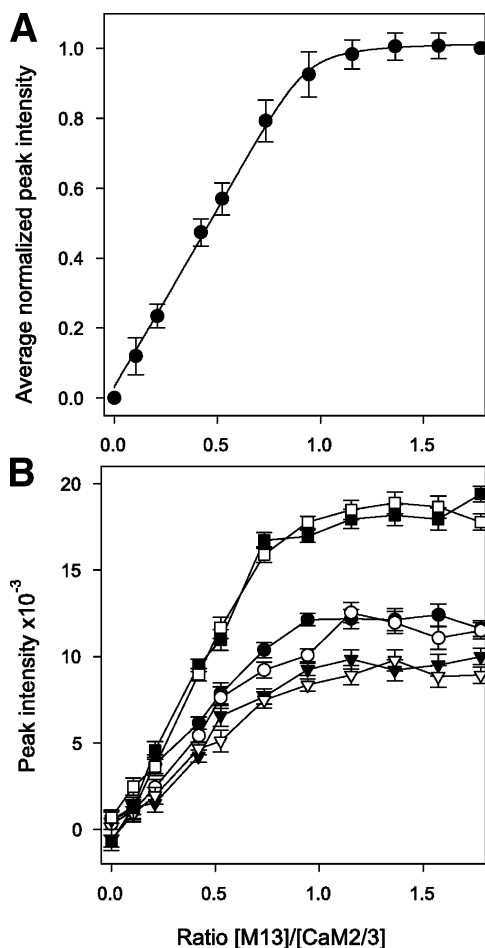
FIGURE 2: Quantitative analysis of the ^{15}N-HSQC monitored titration of ^{15}N-CaM2/3 with unlabeled M13. (A) Average normalized amide peak intensity and standard deviation for residues 48−55, 65−92, and 102−113 of peptide-bound ^{15}N-CaM2/3 plotted vs the M13/CaM2/3 concentration ratio. For amides with double signals, intensities from 1 'a' and 'b' peaks were added together and normalized. Saturation occurs at an equimolar M13/CaM2/3 ratio. The line represents the fit of the data to a single site binding model, with an apparent $K_d = 0.40 \pm 0.05$ μM, using CaLigator (26). (B) Plot of absolute ^{15}N-HSQC peak intensities vs M13/CaM2/3 concentration ratio show that the 'a' and 'b' peaks for three representative residues (F65a (●) and F65b (○), I100a (▲) and I100b (△), and L105a (■) and L105b (□)) in the bound form of ^{15}N-CaM2/3 are of nearly equal intensity at every point during the titration. The lines are present to guide the eye, and intensities were not adjusted for dilution effects.

Specifically, a sphere with the same MW as that of the 1:1 complex would have an S_{max} of ∼1.6 S, whereas that corresponding to a 2:2 complex would have an S_{max} ∼2.3 S (assuming $f/f_0 = 1.2$ due to hydration; asymmetry would reduce these values). Therefore, the CaM2/3-M13 complex exists as an equilibrium between 2:2 and 1:1 species. Alternative species such as a 2:1 CaM2/3-M13 complex are excluded on the basis of the equimolar equivalence point found in the NMR-monitored titrations (Figure 2A).

Following upon this result, equilibrium sedimentation measurements were carried out at three rotor speeds and with CaM2/3 and M13 at 38, 75, or 150 μM each. As summarized in Table 1, the apparent weight-averaged molecular weight of the sample increased with increasing concentrations or reduced rotor speeds. The lowest apparent molecular weight (13.7 kDa) measured is closer to, but still larger than, the expected molecular weight of a 1:1 CaM2/3-M13 complex
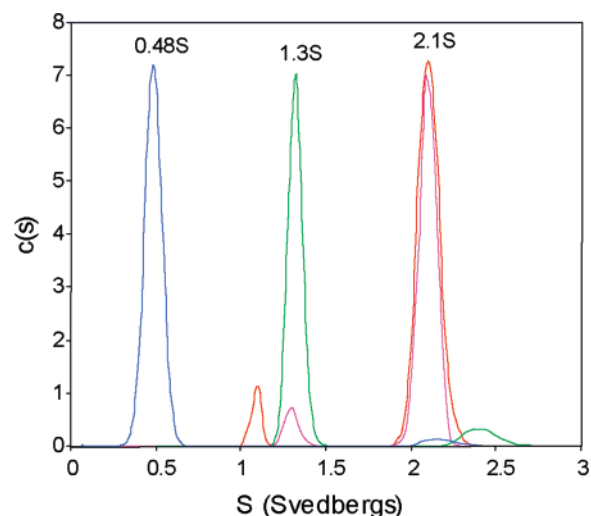
FIGURE 3: Sedimentation velocity c(s) distributions (*55*) for CaM2/3 (75 μM, green), M13 (75 μM, blue), and the CaM2/3-M13 complex (1:1 M13/CaM2/3, each at 75 μM (magenta) or 150 μM (red)) at 20 °C. The M13 peptide sediments predominantly as a momeric species with 0.48 S. CaM2/3 sediments mainly as a monomer (1.34 S) that weakly self-associates as a dimer (∼2.4 S). CaM2/3-M13 sediments predominantly as a 2.1 S species, indicative of an equilibrium between 1:1 and 2:2 complexes (see Table 1).

Table 1: Equilibrium Sedimentation of the CaM2/3-M13 Complex

conc (μM)[a]	apparent molecular weight (kDa) for a given rotor speed (rpm)[b]		
CaM2/3, M13	20,000	30,000	50,000
150, 150	20.1	18.0	14.5
75, 75	17.9	17.7	14.5
38, 38	16.7	16.7	13.7

[a] Total concentration of each species. With $K_d = 0.40$ μM, >90% of CaM2/3 and M13 should exist in equimolar complexes under these conditions. [b] Weight-averaged values. The predicted values are 10.6 kDa for CaM2/3-M13 and 21.3 kDa for (CaM2/3-M13)$_2$.

(10.6 kDa), and the highest (20.1 kDa) is close to that expected for a 2:2 complex (21.3 kDa). Furthermore, the variation of apparent molecular weight with sample concentration reflects the reversibility of the association. This behavior suggests that the higher apparent molecular weight species is due to the self-association of a 1:1 CaM2/3-M13 complex to a 2:2 CaM2/3-M13 complex, rather than the formation of nonspecific aggregates. Moreover, assuming that the CaM2/3 and M13 are fully bound to one another, we were able to globally fit all nine data sets, with SEDPHAT (*33*), for an equilibrium of the form (CaM2/3-M13)$_2$ ⇌ 2(CaM2/3-M13) to obtain an apparent dissociation constant of 130 ± 30 μM.

Concentration-Dependent NMR Spectra of the CaM2/3-M13 Complex. On the basis of the AUC results, the CaM2/3-M13 complex exists predominantly as a 2:2 heterotetramer under the conditions used for the NMR spectral assignments. The observed sets of two equal intensity signals for many residues can thus be explained if the complex is internally asymmetric, with both CaM2/3 and M13 adopting two spectroscopically distinct conformations. To further investigate the stoichiometry of the CaM2/3-M13 complex, we recorded NMR spectra as a function of sample concentration. Between 500 and 100 μM, the ^{15}N-HSQC spectra of ^{15}N-labeled CaM2/3 in the presence of equimolar M13 remained

invariant, without changes in the chemical shifts or relative peak intensities of any amides. However, upon dilution to 25 μM, a new set of dispersed $^1H^N$-^{15}N signals, distinct from those of the tetramer or free CaM2/3, appeared (not shown). Because of the low sample concentration, the new peaks were not assigned. However, for amides with the most dispersed resonances, only single new peaks were observed. Thus, we attribute these signals to a 1:1 CaM2/3-M13 complex. The lack of these signals in samples more concentrated than 100 μM suggests that the actual tetramer—dimer dissociation constant is lower than the fit value of 130 ± 30 μM (i.e., 500 μM total complex would partition as ~70% tetramer and ~30% dimer with this K_d). This discrepancy can be attributed to difficulties in fitting equilibrium ultracentrifugation data to the mixed species present (i.e., free CaM2/3 monomers or possibly dimers and M13 as well as the CaM2/3-M13 complexes).

Secondary Structure of the CaM2/3-M13 Complex. Because of the lack of assignments for the bound M13 peptide and the inability to assign the 'a' and 'b' signals from CaM2/3 to specific conformations, we could not determine the tertiary structure of the CaM2/3-M13 complex. However, the secondary structure of M13 bound CaM2/3 can be accurately predicted using chemical shift information. For example, $^{13}C^\alpha$ chemical shifts move downfield/upfield for residues in α-helices/β-strands relative to a random coil state, whereas the reverse holds for $^{13}C^\beta$ chemical shifts (*38*). On the basis of observed versus reference $^{13}C^\alpha$-$^{13}C^\beta$ chemical shift differences, the two spectroscopically distinguishable forms of the CaM2/3-M13 complex have very similar secondary structures to one another and, with the exception of the linker region, to that of unbound CaM2/3 (Figure 4) (*11*). In particular, four common α-helical regions and two β-strands could be identified in all forms of CaM2/3. This conclusion is also supported by the partial analyses of a ^1H-^{15}N-^1H NOESY-HSQC spectrum, in which diagnostic NOE interactions were detected between I63 $^1H^N$ and I100 $^1H^N$ in free CaM2/3 and in both forms (I63a/b, and I100a/b) of the CaM2/3-M13 complex (data not shown). Together these data confirm that the antiparallel β-sheet between EF-2 and -3 in unbound CaM2/3 is also retained in the M13 complex.

In addition to the invariant α-helices and β-sheet, residues 75−79 in M13-bound CaM2/3 show $^{13}C^\alpha$-$^{13}C^\beta$ chemical shift differences indicative of a new, short α-helical segment. In free CaM2/3, these residues, which correspond to the interdomain linker in native CaM (^{73}ARKMKDTDS^{81}) (*39*), form a flexible loop bridging EF-2 and -3 (*11*). Thus, M13 binding is accompanied by a conformational change in CaM2/3 that includes induction of a helix in the linker sequence.

CaM2/3 Chemical Shift Perturbations due to M13 Binding. The differences in chemical shifts between corresponding nuclei in free and M13-bound CaM2/3 ($\Delta\delta$) provide a qualitative identification of the residues undergoing conformational changes upon complex formation. As shown in Figure 1 and quantitated in Figure 5A, most amides in CaM2/3 exhibited detectable shift perturbations upon complex formation, with an average combined $^1H^N$ and ^{15}N $\Delta\delta$ of 0.27 ± 0.23 ppm. This is suggestive of global tertiary conformational changes. However, the largest amide shift perturbations occur for residues R74, K75, M76, and D78 within the linker sequence and M71, M72, E82, E83, F92,
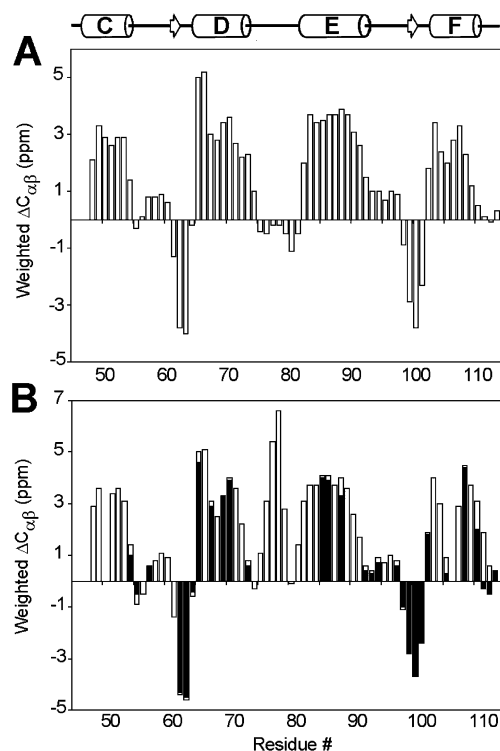

FIGURE 4: Predicted secondary structure of (A) unbound CaM2/3 and (B) M13-bound CaM2/3 determined from weighted $^{13}C^\alpha$ vs $^{13}C^\beta$ chemical shift differences relative to random coil values, $\Delta_{C\alpha\beta(i)}$. Shift differences for residues with two sets of signals in the CaM2/3-M13 complex are plotted together as overlapping black (lower value) and white bars. The residues with positive or negative shift differences are present in α-helixes or β-strands, respectively. The secondary structure of CaM2/3 in the two spectroscopically distinguishable forms of the CaM2/3-M13 complex is essentially the same as that of free CaM2/3, with the addition of a new short helical segment in the hinge region between helices D and E. A schematic of the α-helices (cylinders) and β-strands (arrows) in the NMR-derived structural ensemble of Ca^{2+}-saturated CaM2/3 is also shown.

R106, M109, T110, and N111 in helices D, E, and F. The pronounced amide shift changes for the linker residues 74−78 are consistent with the formation of a helical segment in this region of CaM2/3, as noted above. Spectral differences between CaM2/3 and the CaM2/3-M13 complex were also calculated for the ^1H and ^{13}C nuclei in aromatic residues as well as the alanine methyls. An examination of the aromatic ^{13}C-HSQC spectrum of the CaM2/3-M13 complex showed that the $^1H^{\delta/\epsilon}$ and $^{13}C^{\delta/\epsilon}$ chemical shifts of F65, Y99, and H107 are very similar to those of the unbound protein, whereas F68, F89, and F92 were significantly perturbed (i.e., $\Delta\delta > 0.3$ ppm) (Figure 5B). Adjacent to these latter aromatics, A73 and A88 also exhibited large $^1H^\beta$ and $^{13}C^\beta$ chemical shift changes (i.e., $\Delta\delta > 0.20$ ppm) upon M13 binding (Figure 5C).

The chemical shift perturbations accompanying the formation of the CaM2/3-M13 complex are mapped onto the structure of the unbound protein in Figure 6A and B. These changes could be due either to direct interactions with M13 or a second CaM2/3 within the 2:2 complex or to indirect structural perturbations. Without assignments of the putative 1:1 complex under dilute conditions, the former possibilities cannot be distinguished. With this caveat in mind, it is striking that residues showing the largest amide, aromatic, or alanine methyl chemical shift changes clearly map to a
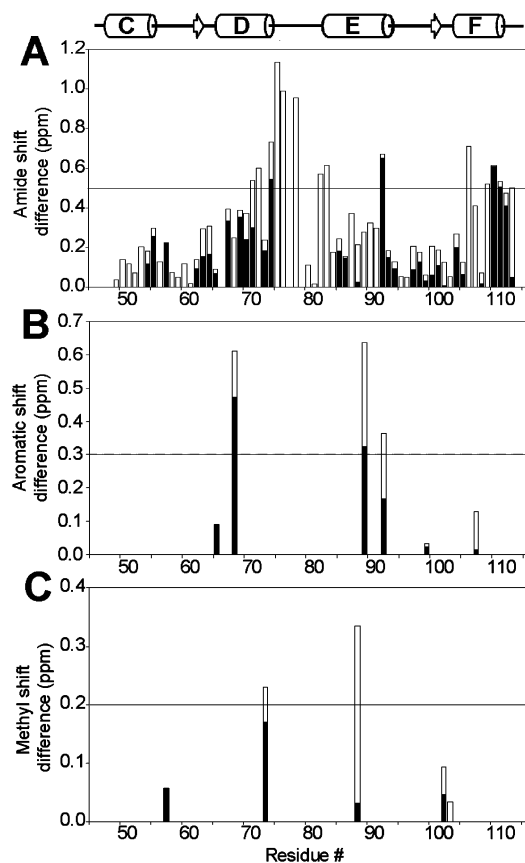
FIGURE 5: Combined (A) amide $^1H^N$-^{15}N, (B) aromatic $^1H^{\delta/\epsilon}$-$^{13}C^{\delta/\epsilon}$, and (C) alanine methyl $^1H^\beta$-$^{13}C^\beta$ chemical shift perturbations of CaM2/3 due to M13 binding, calculated as $\Delta\delta = [(\Delta\delta^1H)^2 + (\Delta\delta I-(\gamma I/\gamma^1H))^2]^{0.5}$. Shift differences for residues with two sets of signals in the CaM2/3-M13 complex are plotted together as overlapping black (lower value) and white bars. The horizontal gray dashed lines indicate the cut-offs (approximately twice the standard deviation of the average change) chosen for defining the residues showing most significant shift changes. These include M71, M72, R74, K75, M76, D78, E82, E83, F92, R106, and M109 from (A), F68, F89, and F92 from (B), and A74 and A88 from (C). These chemical shift perturbations are mapped onto the structure of CaM2/3 in Figure 6.

hydrophobic groove that crosses EF-2 and -3. Analogous to the N- and C-domains of CaM (*6*), this strongly suggests that the M13 peptide binds within this groove via hydrophobic interactions, augmented by additional contacts with flanking polar and charged groups. The chemical shift differences between the 'a' and 'b' double peaks in the complex are plotted similarly onto the surface of unbound CaM2/3 in Figure 6C and D. Many residues showing the largest shift differences cluster within or around this hydrophobic groove, suggesting that the internal asymmetry of the 2:2 heterotetrameric CaM2/3-M13 complex results from two conformations of CaM2/3 and M13 at this binding interface. However, residues giving double resonances are also located on the opposite side of the protein and, most notably, near the *β*-strands bridging EF-2 and -3. This behavior is suggestive of conformational differences between the CaM2/3 molecules in the heterotetramic complex that arise from hinge motions between their constituent EF-hands, a phenomena observed in unbound CaM2/3 (*11*).

CaM2/3-M13 Complex Backbone Dynamics from Amide ^{15}N Relaxation. The global and local backbone dynamic properties of the CaM2/3-M13 complex were investigated
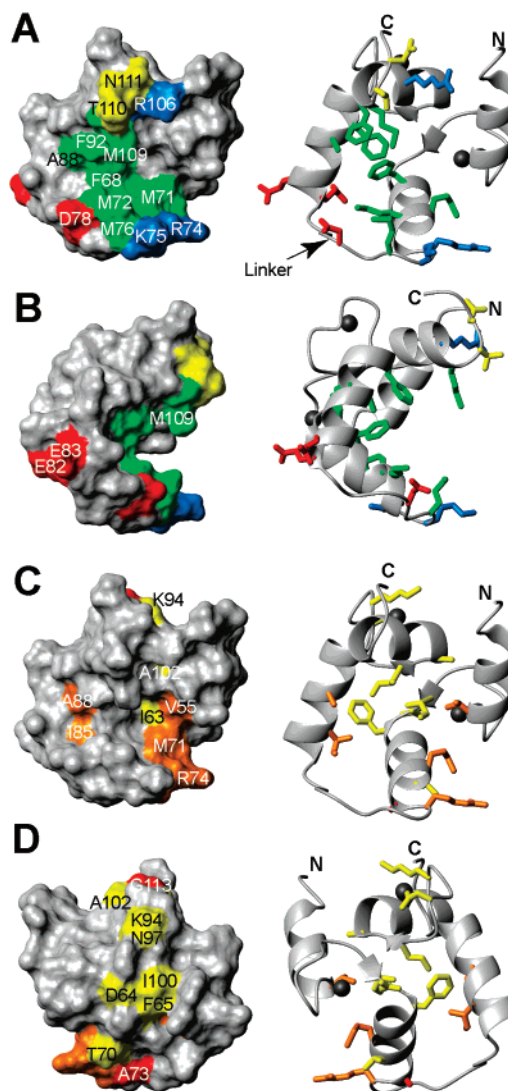

FIGURE 6: Chemical shift perturbations due to M13 binding and differences between double peaks 'a' and 'b' mapped onto the structure of unbound CaM2/3 indicate that the peptide lies within the hydrophobic groove crossing the EF-hands motifs of the protein. In panels A and B (rotated 90° about the vertical axis), residues with the largest amide, aromatic, and alanine methyl shift perturbations upon peptide binding (i.e., above the horizontal cutoff lines in Figure 5) are highlighted on the surface (left) and ribbon (right) drawings of CaM2/3. These include the hydrophobic residues F68, M71, M72, A73, M76, A88, F92, and M109 (green), negatively charged residues D78, E82, and E83 (red), positively charged residues R74, K75, and R106 (blue), and neutral polar residues T110 and N111 (yellow). F89 is obscured by both F65 and F92. In panels C and D (rotated 180°), the chemical shift differences between the 'a' and 'b' double peaks in the CaM2/3-M13 complex are mapped onto the surface of the unbound protein. (Yellow, orange, and red indicate differences greater than 1, 2, and 3 times the standard deviation of the mean shift differences, respectively, for all amide, aromatic, or methyl groups.) Shown is a low-energy model from the NMR-derived structural ensemble of $(Ca^{2+})_2$-CaM2/3 (2HF5.pdb), with black spheres denoting Ca^{2+} ions, rendered using MOLMOL (*56*). Although this representation approximates the structure of M13-bound CaM2/3 with the four *α*-helices of EF-2 and -3 as well as the bridging *β*-sheet present, the flexible linker residues also adopt a helical conformation in the complex.

by ^{15}N T_1, T_2, and heteronuclear $^1H\{^{15}N\}NOE$ relaxation measurements (Figure 7). Consistent with its larger size due to the bound peptide, the CaM2/3-M13 complex exhibits longer average T_1 (0.53 ± 0.07 s) and shorter average T_2
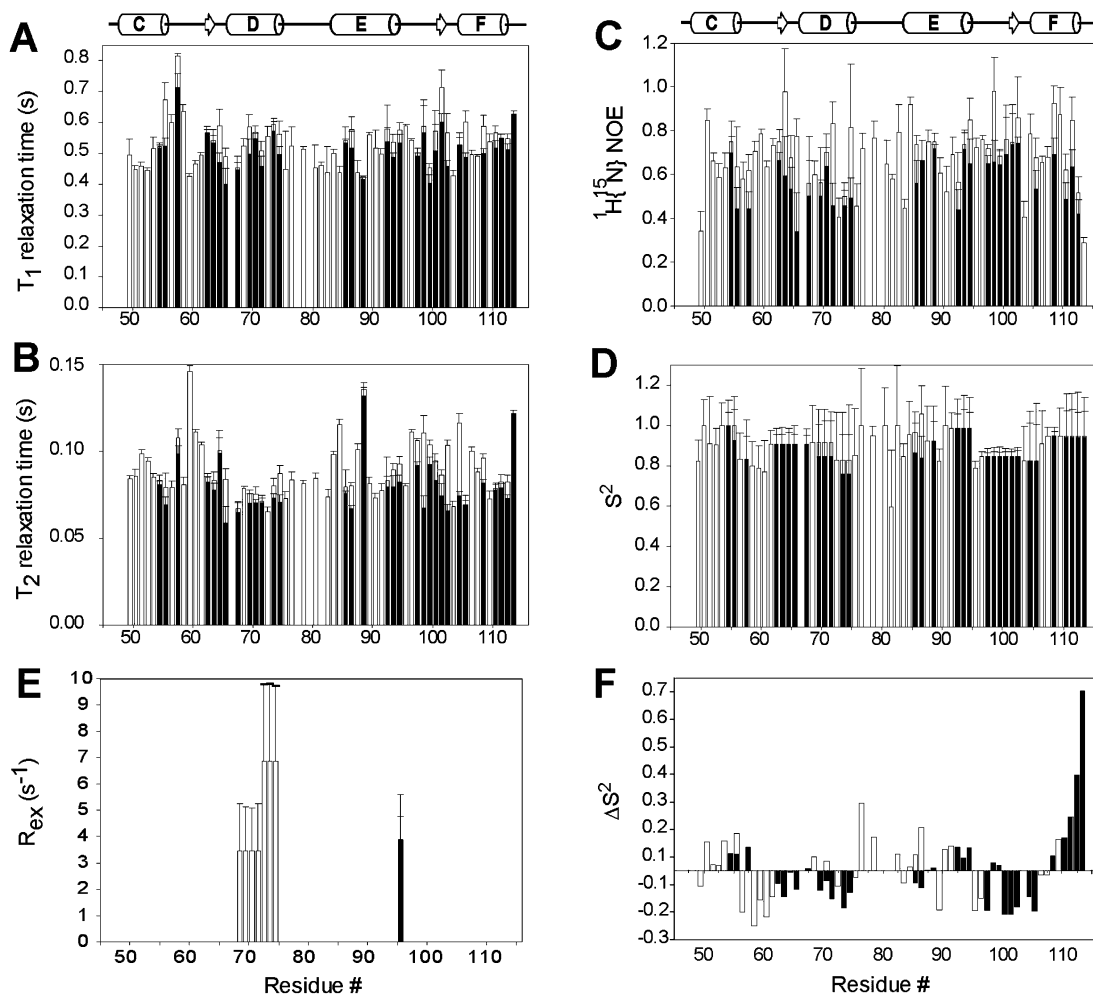
FIGURE 7: Backbone ^{15}N relaxation data and model-free analysis for the CaM2/3-M13 complex. Displayed are the (A) longitudinal (T_1) and (B) transverse (T_2) relaxation times, (C) heteronuclear $^1H\{^{15}N\}$NOE ratios, along with fit (D) isotropic order parameters (S^2), (E) conformational exchange broadening (R_{ex}) parameters, and (F) differences in S^2 between the complexed and free states ($\Delta S^2 = S^2_{CaM2/3-M13} - S^2_{CaM2/3}$). Missing data corresponds to P66 and residues with overlapping or very weak signals. For the residues with double peaks, the parameters are plotted together as overlapping black (lower value) and white (higher value) bars.

(0.085 ± 0.02 s) values than unbound CaM2/3 (average T_1 = 0.41 ± 0.07 s and T_2 = 0.13 ± 0.03 s (*11*)). Excluding residues with T_1/T_2 or heteronuclear $^1H\{^{15}N\}$NOE ratios indicative of conformational exchange or a high degree of internal mobility, analysis of relaxation data yielded an effective correlation time (τ_c) of 7.7 ± 0.1 ns for the global isotropic tumbling of the CaM2/3-M13 complex. This is longer than that measured for CaM2/3 alone (5.1 ± 0.2 ns (*11*)) yet somewhat shorter than that of 9.9 ns reported for a CaM-smMLCK complex at 28 °C (a complex similar in size to the proposed 2:2 CaM2/3-M13 heterotetramer) (*40*). While recognizing that both shape and size contribute to rotational diffusion, the ^{15}N relaxation data may be more consistent with a 1:1 CaM2/3-M13 complex. However, for amides with two sets of $^1H^N$-^{15}N signals in the CaM2/3-M13 complex, the 'a' and 'b' peaks exhibited very similar T_1 and T_2 lifetimes. Therefore, it is unlikely that one set of signals corresponds to a 1:1 complex and the other to a 2:2 complex in slow exchange on the chemical shift time scale, as the higher molecular weight of the latter would systematically yield increased T_1 and decreased T_2 values for one set relative to the other. Rather, the 'a' and 'b' peaks must arise from similar sized and equally populated species, which is most consistent with CaM2/3-M13 existing predominantly as an asymmetric 2:2 complex under the conditions used for relaxation measurements.

The internal dynamic properties of the backbone of CaM2/3 bound to M13 were described using the isotropic Lipari−Szabo model-free formalism in terms of a generalized order parameter S^2 that decreases from 1 to 0 with increased mobility of the amide $^1H^N$-^{15}N (Figure 7D). The CaM2/3-M13 complex exhibits relatively uniform S^2 values of 0.90 ± 0.07, consistent with a well-folded structure. Slightly reduced S^2 values are noted, for example, with residues in the loop regions between helices C/D and E/F of the EF-2 and -3 motifs, respectively. More interestingly, the changes in the order parameters ($\Delta S^2 = S^2_{CaM2/3-M13} - S^2_{CaM2/3}$) of CaM2/3 due to M13 binding are presented in Figure 7F. Most notably, the S^2 values for residues near the C-terminus of the protein, within helices C, E, and F, and within the linker are higher in the complex than in the free protein, indicative of dampened backbone mobility. In the case of the linker, this is consistent with the $^{13}C^\alpha$-$^{13}C^\beta$ secondary chemical shift analyses showing the formation of a helix upon binding (Figure 4). In contrast, the amide order parameters for segments within both EF-hands of CaM2/3 decreased upon complex formation. At face value, this suggests an increase in backbone mobility for some regions of CaM2/3. Alter-
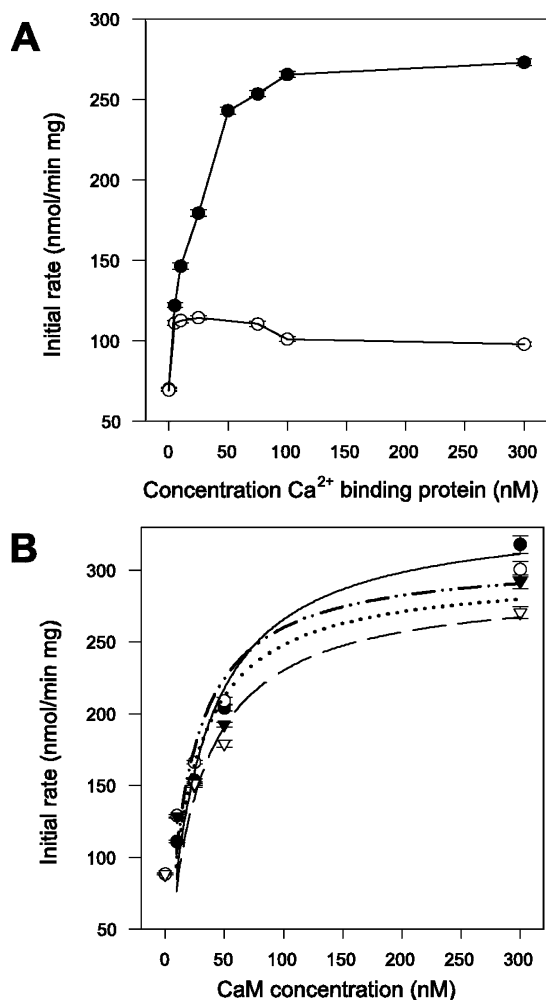
FIGURE 8: CaM2/3 both stimulates calcineurin and inhibits stimulation by CaM. (A) Enzyme stimulation curve showing increasing initial rate of calcineurin phosphatase activity with increasing concentrations of (●) CaM and (○) CaM2/3. (B) CaM competition experiment performed with CaM2/3. Each experimental group consists of a calcineurin stimulation study with 0, 10, 50, and 300 nM CaM in the presence of (—●—) 0, (-..- ○ -..-) 10, (···▼···) 50, and (—▽—) 100 nM of CaM2/3. The curves, fit to the standard Michaelis−Menten equation, show a decrease in the maximum rate of calcineurin phosphatase activity with increasing concentrations of CaM2/3.

natively, this may result from anisotropic diffusion of the CaM2/3-M13 complex (for which a structural model is unavailable) that is not accounted for in the isotropic Lipari−Szabo formalism. Such dynamic changes may also be reflected by the anomalously short T_2 lifetimes measured for residues 68−74 (helix D) of CaM2/3 in its M13-bound, but not unbound, state (*11*). This relaxation behavior is usually the result of conformational exchange broadening (R_{ex}) due to intermediate time scale (ms−μs) motions (Figure 7E). Several of these residues are perturbed upon the binding of CaM2/3 to M13, and thus, their amide relaxation may report mobility of CaM2/3 and/or the M13 peptide at this interfacial region.

Calcineurin Activity Assay. The M13 binding activity displayed by CaM2/3 suggests that it may also retain some of the function of native CaM such as the stimulation of calcineurin phosphatase activity. The results of a phosphatase assay (*36*) confirm that CaM2/3 produces a small, but significant, increase in the activity of calcineurin (Figure 8A).

Furthermore, CaM2/3 also inhibited the stimulation of calcineurin by native CaM. This is evidenced by a CaM2/3 concentration-dependent reduction in the apparent maximal rate of calcineurin phosphatase activity stimulated by CaM (Figure 8B).

DISCUSSION

To investigate the structural and functional diversity possible for EF-hand proteins, we characterized a fragment of CaM composed of EF-2 and -3 and the intervening linker sequence. Although Ca^{2+}-free CaM2/3 is predominantly unfolded, upon binding two equivalents of Ca^{2+}, the protein adopts a structure that is strikingly similar to that of either the N- or C-terminal domain of Ca^{2+}-ligated CaM (*11*). In particular, CaM2/3 has a hydrophobic groove resembling those that mediate the binding of CaM-target sequences to both domains of Ca^{2+}-ligated CaM. Therefore, we hypothesized that the non-natively paired EF-hands of CaM2/3 could also bind such targets. Using NMR spectroscopy, analytical ultracentrifigation, and enzymatic assays, we have confirmed this hypothesis for the M13 peptide and calcineurin.

CaM2/3-M13 Forms an Asymmetric Heterotetramer. ^{15}N-HSQC-monitored titrations revealed that ^{15}N-CaM2/3 binds the M13 peptide with high overall affinity ($K_d = 0.40 \pm 0.05 \mu$M). This dissociation constant is comparable to those of 0.3 and 3 μM reported for the binding of the tryptic N- and C-domain fragments of CaM to skMLCK, respectively (*41*). However, the observed equimolar stoichiometry excludes the possibility that two CaM2/3 molecules associate with one M13, forming an asymmetric 2:1 CaM2/3-M13 complex and thereby recapitulating the roles of the N- and C-domains of CaM. Furthermore, in contrast to CaM, which yields a single M13 complex (*6*), two sets of equally intense amide $^1H^N$-^{15}N and aliphatic/aromatic ^1H-^{13}C signals were observed for many residues in the CaM2/3-M13 complex. The sole tryptophan from M13 also yielded two indole signals, which provides additional evidence against a 2:1 species. Although this spectral doubling could arise from CaM2/3 and M13 forming conformationally distinct 1:1 heterodimers, such a situation seems unlikely because the two species would have to be isoenergetic in order to be present at equal populations.

Complementing these spectroscopic results, AUC data revealed that the CaM2/3-M13 complex exists as an equilibrium between a 1:1 heterodimer and an 2:2 heterotetramer with an apparent dissociation constant of $130 \pm 30 \mu$M. Thus, under the conditions used for most of the NMR experiments, the heterotetramer predominates, and only upon dilution of the complex to 25 μM were a new set of dispersed NMR signals attributable to the heterodimer observed. Although the global isotropic tumbling time (τ_c) of CaM2/3-M13 at 0.5 mM is somewhat shorter than that expected for a 21.3 kDa species (*42*), the fact that the 'a' and 'b' signals for each residue exhibited very similar ^{15}N relaxation properties argues strongly that both arise from similar sized species (i.e., not a mixture of 1:1 and 2:2 oligomers).

Combining the results from the NMR and AUC measurements, we conclude that the CaM2/3-M13 complex adopts two spectroscopically distinct conformations as part of an

internally asymmetric 2:2 heterotetramer. Exchange between these equally populated conformations, and with free CaM2/3, occurs on a time scale longer than seconds, as shown by the distinct chemical shifts of all three species during a titration experiment. Unfortunately, because of spectral overlap and the lack of assignments for the putative heterodimer, we were unable to determine the three-dimensional structure(s) of the CaM2/3-M13 complex(es) by standard NMR methods or to identify the CaM2/3−CaM2/3 interface within the 2:2 species. Thus, the exact nature of the conformational differences leading to the asymmetry of the CaM2/3-M13 complex remains to be established.

M13 Binds to a Hydrophobic Groove in CaM2/3. Chemical shift perturbation mapping demonstrates that the M13 peptide binds to the hydrophobic groove identified in the NMR-derived structure ensemble of CaM2/3 (Figure 6). In particular, the greatest amide, aromatic, and alanine methyl chemical shift changes occur for residues in the linker region and in helices D, E, and F. These residues include F68, M71 M72, A73, M76, A88, F89, F92, and M109, which form a hydrophobic groove spanning EF-2 and -3, as well as R74, K75, D78, E82, E83, R106, T110, and N111, which line the edges of this groove. Thus, as seen for Ca^{2+}-ligated CaM in complex with the same peptide (*6*), it is very likely that M13 binds as an amphipathic helix along this methionine-rich cleft via hydrophobic contacts, augmented with electrostatic and hydrogen bonding interactions to the flanking polar and charged side chains. Note that the M13 peptide is grouped into the 1-5-8-14 class of CaM-binding sequences on the basis of the position of its hydrophobic anchor residues (*43*). Although we have not determined the 3D structure of CaM2/3 bound to M13, the general structural features of the unbound CaM2/3 are most probably retained in the resulting complex(es). Reasons for this include the presence of the hydrophobic binding groove in unbound CaM2/3, the retention of the α-helices and bridging β-sheet between the EF-hands upon complex formation, and the observation that the structures of the N- and C-domains of Ca^{2+}-ligated CaM do not change significantly in the presence of target peptides (*1*, *6*). One notable exception, however, is that residues 75−79 adopt a new small helical segment in CaM2/3-M13 as evident from their $^{13}C^{\alpha}$-$^{13}C^{\beta}$ secondary chemical shifts. In free CaM2/3, these residues form a flexible loop between EF-2 and -3, whereas in native CaM, they are part of the interdomain linker. This linker exists as a long helix in the crystal structure of CaM (*44−46*), and in solution, it is clearly conformationally dynamic (*47*), thereby facilitating the formation of diverse target peptide complexes (*1*). In these complexes, the linker residues generally do not assume any regular secondary structure. However, in a recent X-ray crystallographic analysis of CaM with a peptide fragment corresponding to the CaM-binding site of calcineurin, the linker was found to be helical (*48*). In the case of CaM2/3, M13 binding may lead to a small change in the relative positions of EF-2 and -3 that now accommodates the formation of a helix by the intervening linker residues.

Interaction of CaM2/3 with Calcineurin. In addition to binding the M13 peptide, CaM2/3 has a limited ability to stimulate calcineurin and to inhibit the stimulation of this phosphatase by CaM. In contrast, previous studies with the N- and C-terminal tryptic fragments of CaM have shown

that neither of these fragments can influence the activitiy of calcineurin (*8*).

Similar to the M13 peptide, calcineurin contains a 1-5-8-14 CaM recognition sequence (*1*, *43*). Thus, CaM2/3 may directly bind to the CaM-target site of calcineurin and thereby stimulate its phosphatase activity. However, this effect is significantly less than that observed with CaM, suggesting that CaM2/3 may not efficiently displace the auto-inhibitory domain from the active site of calcineurin because of either reduced binding affinity for or altered structural interactions with its adjacent recognition sequence. Consistent with this hypothesis, CaM2/3 also inhibits the stimulation of calcineurin by CaM. However, as shown in Figure 8B the maximum initial rate of CaM stimulated phosphatase activity of calcineurin decreases with increasing CaM2/3, suggesting an apparent noncompetitive, rather than competitive, mechanism of inhibition. Unfortunately, we were unable to investigate this further by carrying out the calcineurin stimulation assays over a wider range of conditions because high CaM concentrations (>300 nM) alone inhibit the activity of calcineurin. Thus, the mechanism of inhibition and the location of the binding site for CaM2/3 on calcineurin remain to be established.

Diversity of Target Recognition by CaM. CaM2/3 involves the non-native association of EF-2 and -3, and as such is neither optimized for folding or specific target recognition. Despite this, CaM2/3 adopts a Ca^{+2}-dependent structure with peptide binding properties strikingly similar to those of the N- or C-domains of intact CaM. This clearly exemplifies the remarkable plasticity of EF-hand sequences to associate into EF-hand domains and mediate Ca^{2+}-dependent recognition of target proteins. Following the first structural description of CaM complexed with M13 (*6*), an amazing repertoire of possible binding mechanisms have been discovered. These include parallel and antiparallel orientations of target peptides with respect to CaM (*49*) as well as varying stoichiometries such as 1:1 (*6*, *50*), 1:2 (*51*), and 2:2 (*52*) CaM/target−peptide complexes. Examples have also been described where a only single domain of CaM binds to a target (*53*) and where target binding occurs in the presence and absence of Ca^{+2} (*54*). Apo-CaM has even been found as a domain-swapped dimer (*54*). Expanding upon this diversity, CaM2/3-M13 is unusual in existing as an equilibrium between a 1:1 heterodimer and an asymmetric 2:2 heterotetramer. Understanding the exact basis for this unusual asymmetry, which likely results from CaM2/3 and M13 adopting two different, spectroscopically distinct conformations at their binding interfaces, awaits further characterization of related EF-hand domains with additional target sequences.

REFERENCES

1. Yamniuk, A. P., and Vogel, H. J. (2004) Calmodulin's flexibility allows for promiscuity in its interactions with target proteins and peptides, *Mol. Biotechnol. 27*, 33−57.
2. Lewit-Bentley, A., and Rety, S. (2000) EF-hand calcium-binding proteins, *Curr. Opin. Struct. Biol. 10*, 637−643.
3. Klee, C. B. (1988) In *Calmodulin: Molecular Aspects of Cellular Regulation* (Cohen, P., Ed.) pp 35−56, Elsevier Science Publishers, Amsterdam.
4. Zhang, M., Tanaka, T., and Ikura, M. (1995) Calcium-induced conformational transition revealed by the solution structure of apo calmodulin, *Nat. Struct. Biol. 2*, 758−767.
5. Kuboniwa, H., Tjandra, N., Grzesiek, S., Ren, H., Klee, C. B., and Bax, A. (1995) Solution structure of calcium-free calmodulin, *Nat. Struct. Biol. 2*, 768−776.

6. Ikura, M., Clore, G. M., Gronenborn, A. M., Zhu, G., Klee, C. B., and Bax, A. (1992) Solution structure of a calmodulin-target peptide complex by multidimensional NMR, *Science 256*, 632–638.

7. Guerini, D., Krebs, J., and Carafoli, E. (1984) Stimulation of the purified erythrocyte Ca²⁺-ATPase by tryptic fragments of calmodulin, *J. Biol. Chem. 259*, 15172–15177.

8. Newton, D. L., Oldewurtel, M. D., Krinks, M. H., Shiloach, J., and Klee, C. B. (1984) Agonist and antagonist properties of calmodulin fragments, *J. Biol. Chem. 259*, 4419–4426.

9. Kuznicki, J., Grabarek, Z., Brzeska, H., Drabikowski, W., and Cohen, P. (1981) Stimulation of enzyme activities by fragments of calmodulin, *FEBS Lett. 130*, 141–145.

10. Wolff, J., Newton, D. L., and Klee, C. B. (1986) Activation of *Bordetella pertussis* adenylate cyclase by the carboxyl-terminal tryptic fragment of calmodulin, *Biochemistry 25*, 7950–7955.

11. Lakowski, T. M., Lee, G. M., Okon, M., Reid, R. E., and McIntosh, L. P. (2007) Calcium-induced folding of a fragment of calmodulin composed of EF-hands 2 and 3, *Protein Sci. 16*, 1119–1132.

12. Rink, H. (1987) Solid-phase synthesis of protected peptide fragments using a trialkoxy-diphenyl-methyl ester resin, *Tetrahedron Lett. 28*, 3787–3790.

13. Dourtoglou, V., Gross, B., Lambropoulou, V., and Zioudrou. (1984) O-Benzotriazolyl-N,N,N′,N′ tetramethyluronium hexafluro-phosphate as a coupling reagent for the synthesis of peptides of biological interest, *Synthesis 7*, 572–574.

14. King, D. S., Fields, C. G., and Fields, G. B. (1990) A cleavage method which minimizes side reactions following Fmoc solid phase peptide synthesis, *Int. J. Pept. Protein Res. 36*, 255–266.

15. Procyshyn, R. M., and Reid, R. E. (1994) An examination of glutamic acid in the -X chelating position of the helix-loop-helix calcium binding motif, *Arch. Biochem. Biophys. 311*, 425–429.

16. Don, R. H., Cox, P. T., Wainwright, B. J., Baker, K., and Mattick, J. S. (1991) 'Touchdown' PCR to circumvent spurious priming during gene amplification, *Nucleic Acids Res. 19*, 4008.

17. Grzesiek, S., and Bax, A. (1992) Correlating backbone amide and side chain resonances in larger proteins by multiple relayed triple resonance NMR, *J. Am. Chem. Soc. 114*, 6291–6293.

18. Grzesiek, S., and Bax, A. (1993) Amino acid type determination in the sequential assignment procedure of uniformly ¹³C/¹⁵N-enriched proteins, *J. Biomol. NMR 3*, 185–204.

19. Logan, T. M., Olejniczak, E. T., Xu, R. X., and Fesik, S. W. (1992) Side chain and backbone assignments in isotopically labeled proteins from two heteronuclear triple resonance experiments, *FEBS Lett. 314*, 413–418.

20. Yamazaki, T., Forman-Kay, J. D., and Kay, L. E. (1993) Two-dimensional NMR experiments for correlating ¹³Cβ and ¹Hδ/ε chemical shifts of aromatic residues in 13C labeled proteins via scalar couplings, *J. Am. Chem. Soc. 115*, 11054–11055.

21. Delaglio, F., Grzesiek, S., Vuister, G. W., Zhu, G., Pfeifer, J., and Bax, A. (1995) NMRPipe: a multidimensional spectral processing system based on UNIX pipes, *J. Biomol. NMR 6*, 277–293.

22. Goddard, T. D., and Kneeler, D. G. (1999) *Sparky*, University of California, San Francisco, San Francisco, CA.

23. Wishart, D. S., Sykes, B. D., and Richards, F. M. (1992) The chemical shift index: a fast and simple method for the assignment of protein secondary structure through NMR spectroscopy, *Biochemistry 31*, 1647–1651.

24. Wishart, D. S., Sykes, B. D., and Richards, F. M. (1991) Relationship between nuclear magnetic resonance chemical shift and protein secondary structure, *J. Mol. Biol. 222*, 311–333.

25. Yap, K. L., and Tomomori, C. (1999) *CSI*, University of Toronto, Toronto, Canada.

26. Andre, I., and Linse, S. (2002) Measurement of Ca²⁺-binding constants of proteins and presentation of the CaLigator software, *Anal. Biochem. 305*, 195–205.

27. Farrow, N. A., Zhang, O., Szabo, A., Torchia, D. A., and Kay, L. E. (1995) Spectral density function mapping using ¹⁵N relaxation data exclusively, *J. Biomol. NMR 6*, 153–162.

28. Farrow, N. A., Muhandiram, R., Singer, A. U., Pascal, S. M., Kay, C. M., Gish, G., Shoelson, S. E., Pawson, T., Forman-Kay, J. D., and Kay, L. E. (1994) Backbone dynamics of a free and phosphopeptide-complexed Src homology 2 domain studied by ¹⁵N NMR relaxation, *Biochemistry 33*, 5984–6003.

29. Dosset, P., Hus, J. C., Blackledge, M., and Marion, D. (2000) Efficient analysis of macromolecular rotational diffusion from heteronuclear relaxation data, *J. Biomol. NMR 16*, 23–28.

30. Tjandra, N., Feller, S. E., Richard, W. P., and Bax, A. (1995) Rotational diffusion anisotropy of human ubiquitin from ¹⁵N NMR relaxation, *J. Am. Chem. Soc 117*, 12562–12566.

31. Jeffrey, L., and Yphantis, D. (2005) *WinMatch*, National Analytical Ultracentrifugation Facility, University of Connecticut, Storrs, CT.

32. Laue, T. M., Shah, B. D., Ridgeway, T. M., and Pelletier, S. L. (1992) *Analytical Ultracentrifugation in Biochemistry and Polymer Science*, Royal Society of Chemistry, Cambridge, U.K.

33. Schuck, P. (2003) On the analysis of protein self-association by sedimentation velocity analytical ultracentrifugation, *Anal. Biochem. 320*, 104–124.

34. Schuck, P., Perugini, M. A., Gonzales, N. R., Howlett, G. J., and Schubert, D. (2002) Size-distribution analysis of proteins by analytical ultracentrifugation: strategies and application to model systems, *Biophys. J. 82*, 1096–1111.

35. Mondragon, A., Griffith, E. C., Sun, L., Xiong, F., Armstrong, C., and Liu, J. O. (1997) Overexpression and purification of human calcineurin alpha from *Escherichia coli* and assessment of catalytic functions of residues surrounding the binuclear metal center, *Biochemistry 36*, 4934–4942.

36. Klee, C. B., Krinks, M. H., Manalan, A. S., Cohen, P., and Stewart, A. A. (1983) Isolation and characterization of bovine brain calcineurin: a calmodulin-stimulated protein phosphatase, *Methods Enzymol. 102*, 227–244.

37. Farrow, N. A., Zhang, O., Forman-Kay, J. D., and Kay, L. E. (1994) A heteronuclear correlation experiment for simultaneous determination of ¹⁵N longitudinal decay and chemical exchange rates of systems in slow equilibrium, *J. Biomol. NMR 4*, 727–734.

38. Wishart, D. S., and Sykes, B. D. (1994) The ¹³C chemical-shift index: a simple method for the identification of protein secondary structure using ¹³C chemical-shift data, *J. Biomol. NMR 4*, 171–180.

39. Fiorin, G., Biekofsky, R. R., Pastore, A., and Carloni, P. (2005) Unwinding the helical linker of calcium-loaded calmodulin: A molecular dynamics study, *Proteins 61*, 829–839.

40. Lee, A. L., Sharp, K. A., Kranz, J. K., Song, X. J., and Wand, A. J. (2002) Temperature dependence of the internal dynamics of a calmodulin-peptide complex, *Biochemistry 41*, 13814–13825.

41. Persechini, A., McMillan, K., and Leakey, P. (1994) Activation of myosin light chain kinase and nitric oxide synthase activities by calmodulin fragments, *J. Biol. Chem. 269*, 16148–16154.

42. Daragan, V. A., and Mayo, K. H. (1997) Motional model analyses of protein and peptide dynamics using ¹³C and ¹⁵N NMR relaxation, *Prog. Nucl. Magn. Reson. Spectrosc. 31*, 63–105.

43. Yap, K. L., Kim, J., Truong, K., Sherman, M., Yuan, T., and Ikura, M. (2000) Calmodulin target database, *J. Struct. Funct. Genomics 1*, 8–14.

44. Chattopadhyaya, R., Meador, W. E., Means, A. R., and Quiocho, F. A. (1992) Calmodulin structure refined at 1.7 Å resolution, *J. Mol. Biol. 228*, 1177–1192.

45. Babu, Y. S., Bugg, C. E., and Cook, W. J. (1988) Structure of calmodulin refined at 2.2 Å resolution, *J. Mol. Biol. 204*, 191–204.

46. Wilson, M. A., and Brunger, A. T. (2000) The 1.0 Å crystal structure of Ca⁽²⁺⁾-bound calmodulin: an analysis of disorder and implications for functionally relevant plasticity, *J. Mol. Biol. 301*, 1237–1256.

47. Barbato, G., Ikura, M., Kay, L. E., Pastor, R. W., and Bax, A. (1992) Backbone dynamics of calmodulin studied by ¹⁵N relaxation using inverse detected two-dimensional NMR spectroscopy: the central helix is flexible, *Biochemistry 31*, 5269–5278.

48. Ye, Q., Li, X., Wong, A., Wei, Q., and Jia, Z. (2006) Structure of calmodulin bound to a calcineurin peptide: a new way of making an old binding mode, *Biochemistry 45*, 738–745.

49. Osawa, M., Tokumitsu, H., Swindells, M. B., Kurihara, H., Orita, M., Shibanuma, T., Furuya, T., and Ikura, M. (1999) A novel target recognition revealed by calmodulin in complex with Ca²⁺-calmodulin-dependent kinase kinase, *Nat. Struct. Biol. 6*, 819–824.

50. Meador, W. E., Means, A. R., and Quiocho, F. A. (1992) Target enzyme recognition by calmodulin: 2.4 Å structure of a calmodulin-peptide complex, *Science 257*, 1251–1255.

51. Yap, K. L., Yuan, T., Mal, T. K., Vogel, H. J., and Ikura, M. (2003) Structural basis for simultaneous binding of two carboxy-

terminal peptides of plant glutamate decarboxylase to calmodulin, *J. Mol. Biol. 328*, 193−204.

52. Schumacher, M. A., Rivard, A. F., Bachinger, H. P., and Adelman, J. P. (2001) Structure of the gating domain of a Ca^{2+}-activated K^+ channel complexed with Ca^{2+}/calmodulin, *Nature 410*, 1120−1124.

53. Elshorst, B., Hennig, M., Forsterling, H., Diener, A., Maurer, M., Schulte, P., Schwalbe, H., Griesinger, C., Krebs, J., Schmid, H., Vorherr, T., and Carafoli, E. (1999) NMR solution structure of a complex of calmodulin with a binding peptide of the Ca^{2+} pump, *Biochemistry 38*, 12320−12332.

54. Schumacher, M. A., Crum, M., and Miller, M. C. (2004) Crystal structures of apocalmodulin and an apocalmodulin/SK potassium channel gating domain complex, *Structure 12*, 849−860.

55. Gill, S. C., and von Hippel, P. H. (1989) Calculation of protein extinction coefficients from amino acid sequence data, *Anal. Biochem. 182*, 319−326.

56. Koradi, R., Billeter, M., and Wuthrich, K. (1996) MOLMOL: a program for display and analysis of macromolecular structures, *J. Mol. Graphics 14,* 51−55.